Report of Transnational Access Projects

Project ID: C3-TA3-82-1-5

Principal investigator: Nadine Haaf, Karlsruhe Institute of Technology

Project team: Jerome Azzola, Karlsruhe Institute of Technology

Project title: Electric Self-Potential and Fiber-Optic Monitoring of Fluid-Driven Fault Dynamics in the BEACH Experiment

Project acronym: ESPF

Hosting installation: BedrettoLab testbed (TA3-82-1)

Hosting team: Liliana Vargas Meleza, Marian Hertrich, Antonio Rinaldi, Frederick Massin, Pascal Edme, Mathilde Wimez, Valentin Gischig, Marco Bertoldi, Erminio Moltelini.

Period of access: Aug-Sep 2025 Remote planning sessions; 13-24 October 2025 Visit and Sensor deployment; Dec 2025-Feb 2026 Remote access

Report of activities:

This project aims at monitoring electric self-potential (SP) signals during fluid injection to investigate fluid-induced fault activation. The goal is to correlate SP anomalies with seismic, strain, and temperature data acquired from fiber optic sensing (DAS, DSS, DTS). This integration of data types will improve the understanding of geomechanical responses and the role of fluid movement in fault behaviour. In total, 9 electrodes (Pb/PbCl2 PMS9000 non-polarizable electrodes (SDEC, France) filled with NaCl saturated solution and a CR-6 data logger from Campbell Scientific) were installed in the Geothermal Testbed at the BedrettoLab: 8 short boreholes (30 cm) were drilled to instal electrodes along the tunnel wall; 1 electrode was deployed inside a borehole. Continuous data acquisition started on 2025-11-05 and ended on 2025-12-18. Data processing concluded on 2026-02-23. The self-potential data has been analysed jointly with the DTS measurements acquired by the BedrettoLab team.

Project outcomes:

The self-potential dataset is available at DOI: https://doi.org/10.3929/ethz-c-000801804. Data are distributed under CC-BY 4.0 license.

DAS data will be distributed by SED EIDA Node and the EPOS platform under the BedrettoLab Field-Scale Laboratory of the TCS MSL, after the service has been fully integrated (expected Sep 2026).

Geo-INQUIRE is funded by the European Commission under project number 101058518 within the HORIZON-INFRA-2021-SERV-01 call

has been deposited in GFZ Data Services to ensure integration to EPOS MSL Data Catalogue. A Jupyter notebook will be produced and integrated into EPOS Data Portal as a "Scientific Example".

1 Dataset Description

1.1 Self-potential

The dataset comprises self-potential (SP) time series acquired during the BEACH hot-water injection experiment at the Bedretto Underground Laboratory between 26 October and 18 December 2025. The present data release focuses on the injection-related monitoring period and contains the SP measurements used for the analyses presented in this report. Data are provided in millivolts (mV) together with UTC timestamps.

Measurements were recorded using permanently installed $Pb/PbCl_2$ non-polarizable electrodes connected to a multichannel data logger. During acquisition, electrode S95 served as the reference electrode. The measurement system internally subtracted the reference signal, such that all recorded values represent electrical potential differences relative to N95 (ΔV = Velectrode − VN95). Consequently, no additional reference correction was applied during post-processing.

Within the dataset, logger channels SE1–SE8 correspond to the installed field electrodes as follows: SE1 = S32, SE2 = S18, SE3 = S1, SE4 = N1, SE5 = N18, SE6 = N32, SE7 = B60, and SE8 = N95. The electrodes are distributed along the tunnel axis and referenced to the injection borehole ST1 (see Figure 1-1). Their positions relative to ST1 are N1 (+1.8 m), N18 (+18.13 m), N32 (+34.65 m), B60 (+49.5 m), N95 (+99.5 m), S1 (−1.7 m), S18 (−15.60 m), S32 (−34.50 m), and S95 (−99.5 m). Positive distances indicate the northward direction along the tunnel, whereas negative distances indicate the southward direction.

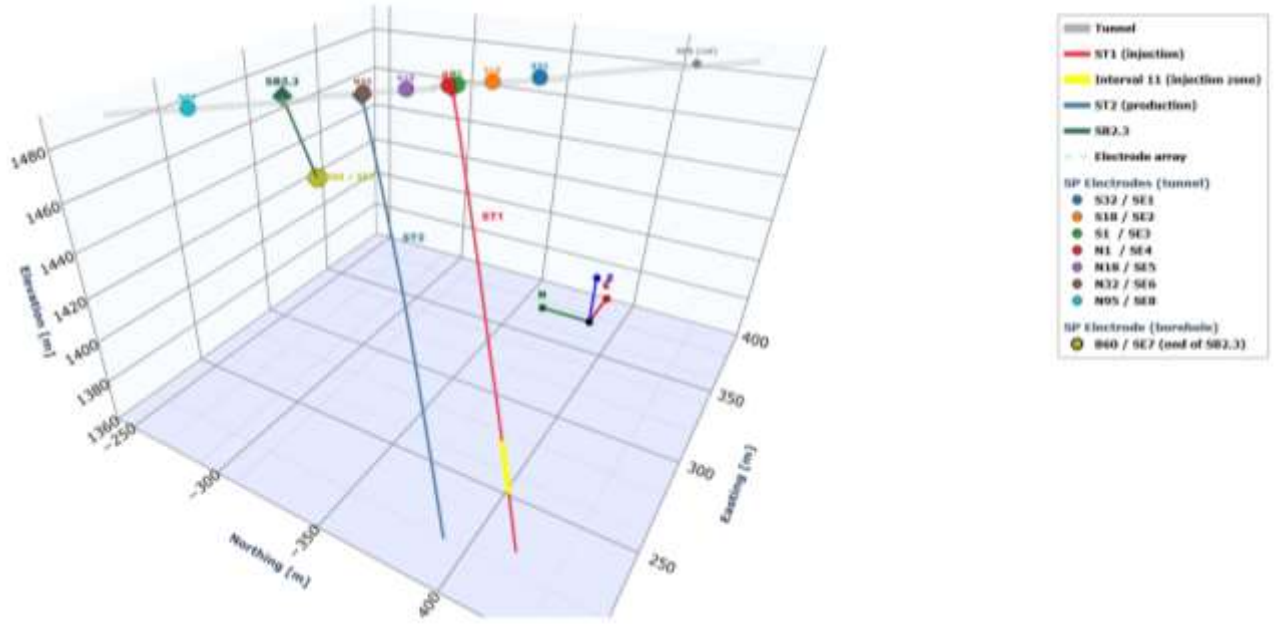

Figure 1-1: Three-dimensional overview of the BedrettoLab geothermal testbed showing the tunnel, the injection borehole ST1 (red), the production borehole ST2 (blue), and monitoring borehole SB2.3 (green). The yellow segment marks Injection Interval 11 within ST1. Self-potential (SP) electrodes installed along the tunnel wall (SE1–SE8) and the borehole electrode B60 (SE7) at the end of SB2.3 are indicated by colored markers.

Geo-INQUIRE is funded by the European Commission under project number 101058518 within the HORIZON-INFRA-2021-SERV-01 call

Figure 1-2: Overview of the BEACH self-potential dataset showing raw SP signals (5 min median, faint lines) and 4 h median SP signals (thick lines) for all eight electrodes. Injection pressure (red) and flow rate (blue) are shown on the secondary axis.

1.2 Fiber optic sensing

Fiber optic sensing data acquired during the BEACH injection experiments were recorded by the hosting team and made available after acquisition according to the data report (Staub et al., 2025). Distributed Acoustic Sensing (DAS) measurements were made available via FDSN web services. During the BEACH injection experiment, DAS data were continuously streamed and distributed through FDSN web services with a temporal sampling frequency of 2000 Hz (after 2025-11-04) and a spatial sampling interval of 16 m for fiber optic cables installed in boreholes MB3 (19 DAS channels), MB5 (27 channels), and MB8 (30 channels) (see Figure 2-2). **However, subsequent analysis of the acquired dataset revealed an error in the mapping of DAS channels along the fiber-optic cables, significantly limiting the interpretation of the measurements and preventing a fully reliable spatial analysis of the recorded wavefield.**

Distributed Temperature Sensing (DTS) data was made available through the data report (Staub et al., 2025) for MB1, MB3, MB4, MB5, MB7, MB8, ST1, ST2, the Rigola and the Bedretto tunnel itself. A measurement was conducted every 10 minutes during the hot injection. In borehole ST2, only the top 250m of the total 350 m are monitored due to an installation error. Distributed Strain Sensing (DSS) data was measured with a spatial resolution of 1m during the hot injection, in boreholes MB4-MB5-MB7-MB8.

2 Data processing

2.1 Self-potential

The raw SP time series were recorded at a sampling interval of 60 s. The data are affected by electromagnetic interference generated by train traffic in the nearby Gotthard Base Tunnel. This disturbance appears as broadband, non-stationary noise with amplitudes reaching up to ±200 mV and a clear diurnal pattern corresponding to train operation hours. Since the disturbance overlaps with the expected injection-related SP signals at periods ranging from minutes to several hours, conventional frequency filtering is not suitable because it would also attenuate signals of interest.

To separate train-related noise from the SP signal, a three-step processing workflow was applied. First, each SP channel was decomposed into intrinsic mode functions (IMFs) using CEEMDAN (Complete Ensemble Empirical Mode Decomposition with Adaptive Noise; Torres et al., 2011). CEEMDAN decomposes the signal into oscillatory components of different characteristic periods without requiring predefined filter parameters.

Second, each IMF was evaluated using a diurnal power ratio, defined as the mean instantaneous power during daytime hours (06:00–22:00) divided by the mean instantaneous power during nighttime hours (22:00–06:00). IMFs with a diurnal power ratio greater than 1.4 were interpreted as being dominated by train-related noise and combined into a channel-specific noise estimate. IMFs with a ratio of 1.4 or lower were retained as potential geophysical signal components.

Finally, a weighted Common Mode Rejection (CMR) approach was applied to remove spatially coherent noise that remained after the CEEMDAN decomposition. Noise estimates from all tunnel electrodes (SE1–SE6 and SE8) were combined into a common reference signal. Individual channel contributions were weighted according to the inverse RMS amplitude and limited to a maximum contribution of 15 % to avoid dominance by a single electrode. The resulting common noise estimate was then subtracted from each channel.

The combined CEEMDAN-CMR processing reduced the RMS amplitude by approximately 20–63 % across the tunnel electrodes SE1–SE6. Figure 2-1 shows the power spectral densities before and after processing.

Geo-INQUIRE is funded by the European Commission under project number 101058518 within the HORIZON-INFRA-2021-SERV-01 call

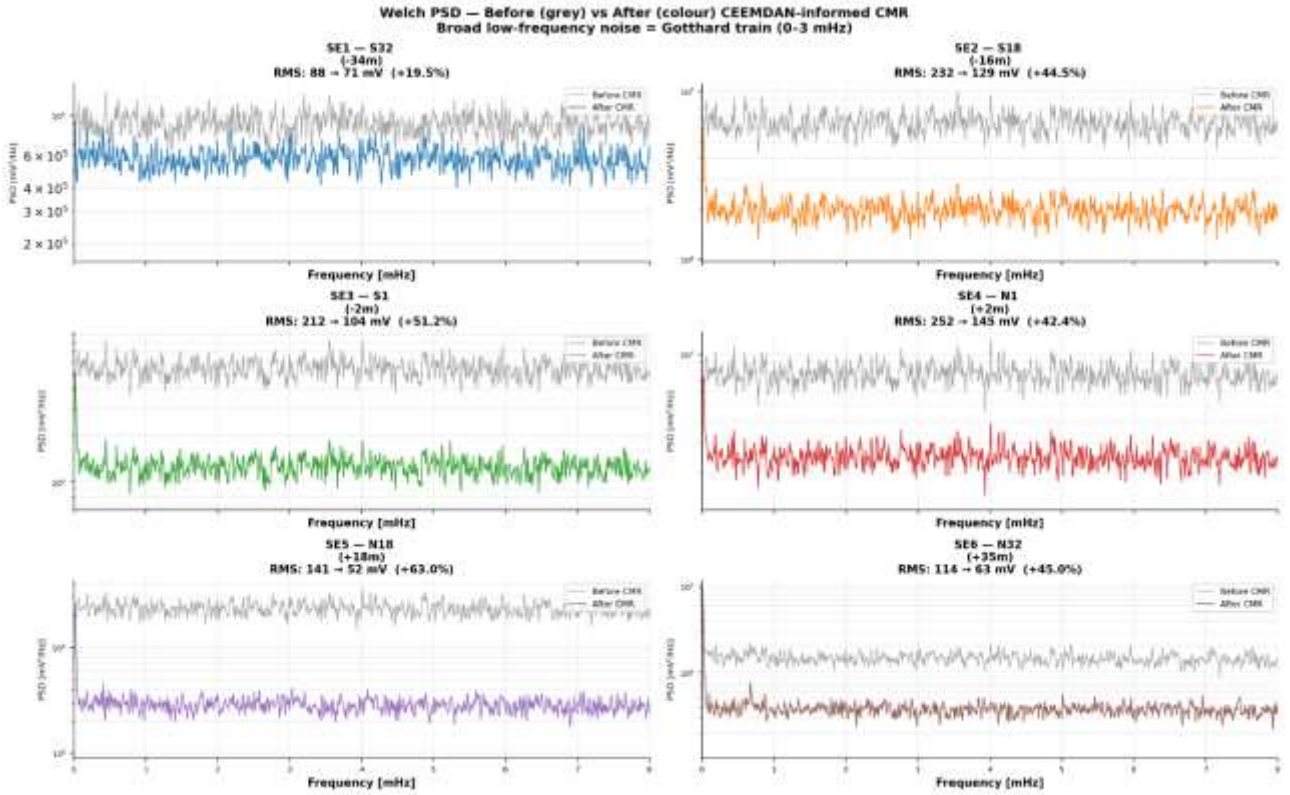

Figure 2-1: Power spectral densities of the SP signals before (grey) and after (coloured) CEEMDAN-informed CMR processing for tunnel electrodes SE1–SE6.

The SP anomaly is defined as $\Delta SP(t) = SP_{4h}(t) - \text{mean}(SP_{4h}$ during Background phase), where SP_{4h} denotes the 4-hour resampled median of the CMR-processed signal and the Background phase (12–24 November 2025, pumps off) serves as the undisturbed reservoir reference. This resolution suppresses residual train noise while preserving the temporal structure of the injection signal, which varies on timescales of hours to days. All figures in this report use this 4-hour median consistently.

2.2 Fiber optic sensing

2.2.1 Key point of the analysis

Despite the limitations outlined above, a main focus in the analysis of fiber optic sensing data was on DAS data. DAS effectively emulates a dense seismic array from a single interrogator unit, enabling the application of array-processing approaches and providing dense spatial sampling of the seismic wavefield within the monitoring volume. In view of the temporal sampling of the data, sensitivity is possible over a broad frequency range, which makes it possible to analyze the imprint of various phenomena, from quasi-static changes to microseismic events across a range of magnitudes. Hence, the analysis focused on two aspects:

1. Evaluating the contribution of DAS measurements to microseismic monitoring during injection operations.

2. Investigating the potential of low-frequency DAS measurements (LF-DAS) for tracking the influence of fracture flow within the instrumented boreholes.

2.2.2 Data analysis

With regards to focus 1), the analysis considered induced events from the seismic catalog (Figure 2-2) occurring after the increase of the DAS sampling frequency to 2000 Hz. Among the largest events in this subset, earthquakes with magnitudes Mw −2.61 and Mw −2.88 were identified in the DAS recordings (see Figure 2-3 and Figure 2-4). Wavefield propagation along the fiber could be observed over source–receiver distances of up to approximately 60 m. However, errors in the mapping of DAS channels prevent a more detailed spatial analysis of the recorded wavefield. Sensitivity to lower-magnitude events is limited by the achievable temporal sampling frequency, whereas the detectability of more distant events is primarily constrained by SNR approaching the instrumental noise floor, dominated by electronic noise and laser phase noise intrinsic to the DAS interrogator system. Despite these limitations, the observations demonstrate that DAS can represent a valuable component of borehole seismic monitoring systems in the context of underground research laboratories, providing dense spatial coverage and high receiver density from a single sensing unit.

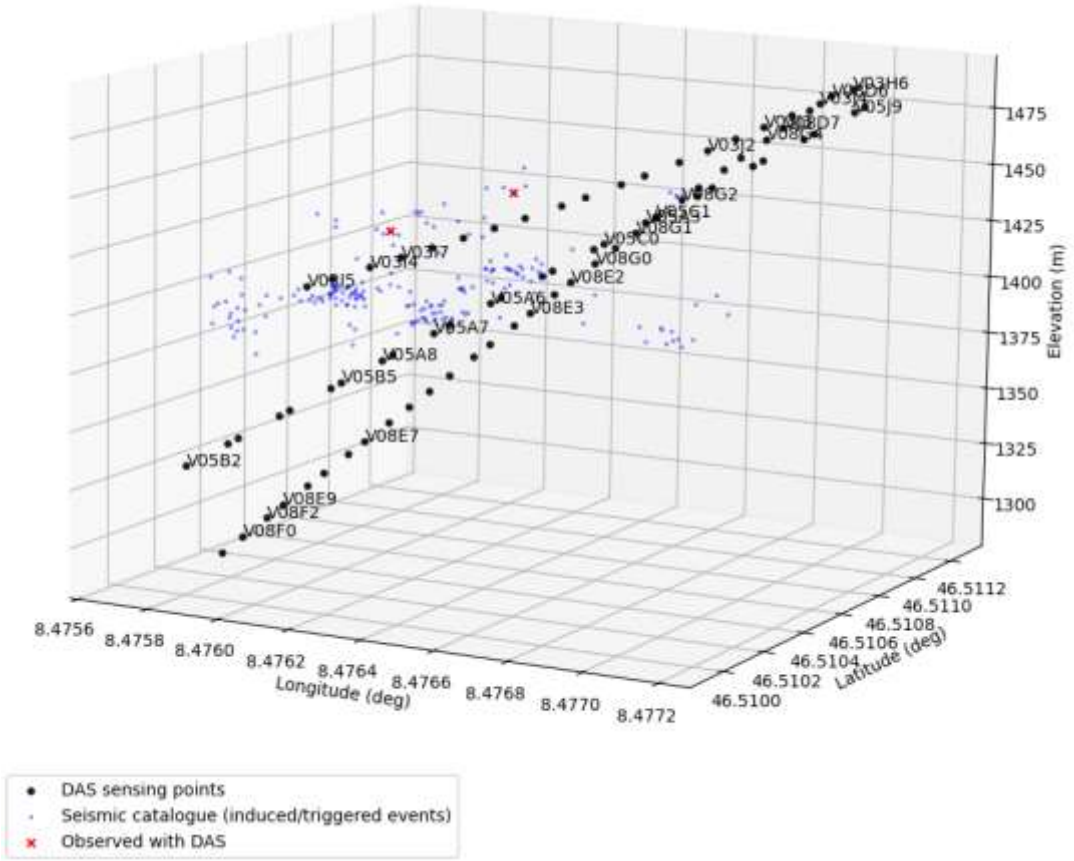

Figure 2-2: black dots indicate DAS sensing points along the borehole trajectory, while blue dots represent induced or triggered seismic events from the seismic catalogue. Red crosses mark events observed with DAS measurements. Axes show longitude, latitude, and elevation coordinates. The figure illustrates the spatial relationship between the DAS array geometry and the detected microseismicity within the geothermal reservoir.

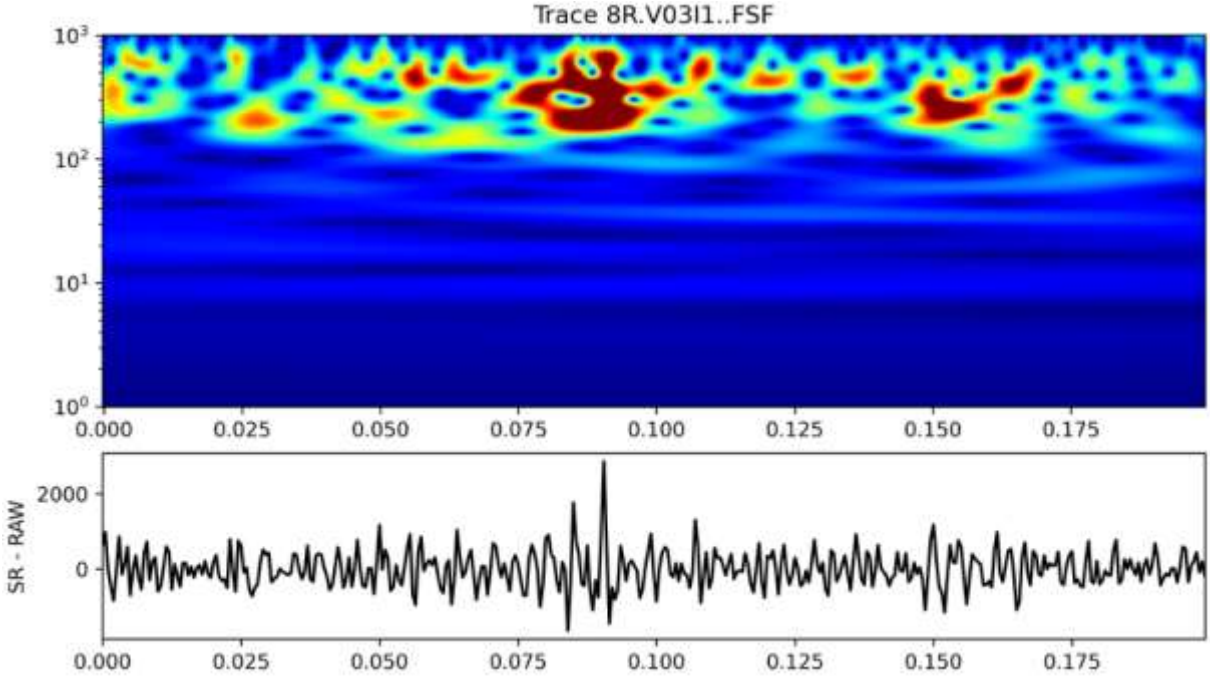

Figure 2-3: time–frequency representation and waveform of a DAS-recorded seismic trace. Top panel: spectrogram of trace 8R.V03I1..FSF showing the temporal evolution of spectral amplitudes over the analyzed frequency range. Bottom panel: corresponding raw strain-rate waveform in the time domain, without filtering.

Geo-INQUIRE is funded by the European Commission under project number 101058518 within the HORIZON-INFRA-2021-SERV-01 call

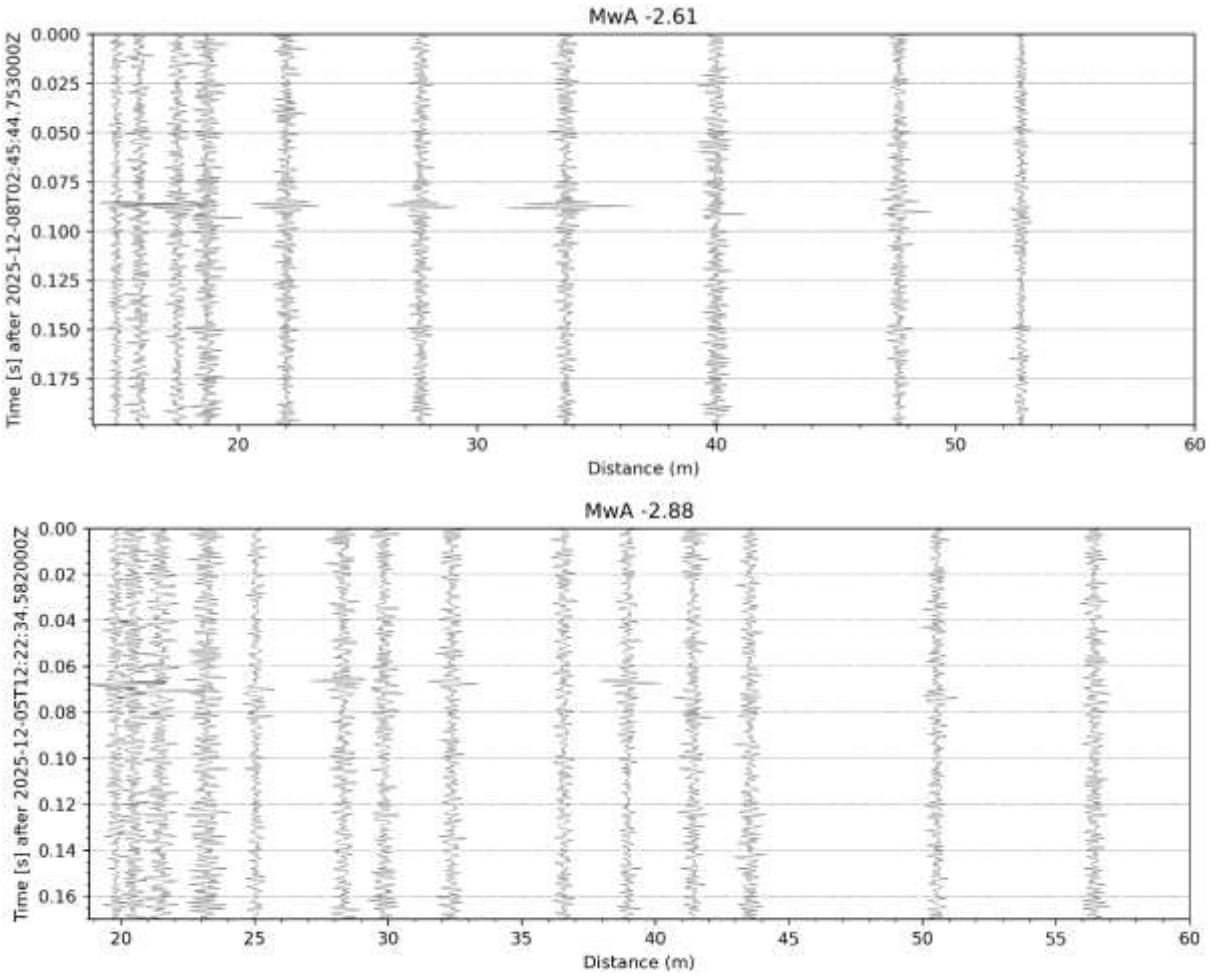

Figure 2-4: for two identified microseismic events in the target volume, the figure displays strain-rate waveforms as a function of distance along the DAS array and time after the event origin time. Distinct coherent arrivals can be observed across multiple sensing channels, illustrating the spatial propagation of seismic wave energy recorded by the distributed acoustic sensing system.

With regards to focus 2), the analysis focused on strain variations recorded at low frequencies, at periods longer than 1 s. Power spectral densities were computed in sliding time windows for each available DAS channel, and the temporal evolution of spectral energy below 1 Hz was evaluated. These temporal variations were subsequently compared with Distributed Strain Sensing (DSS) measurements acquired along the same boreholes. However, due to the false mapping of DAS channels along the fiber-optic cable, the interpretation of the LF-DAS measurements remained limited, and no robust correlation between LF-DAS observations and in particular DSS strain variations could be conclusively established.

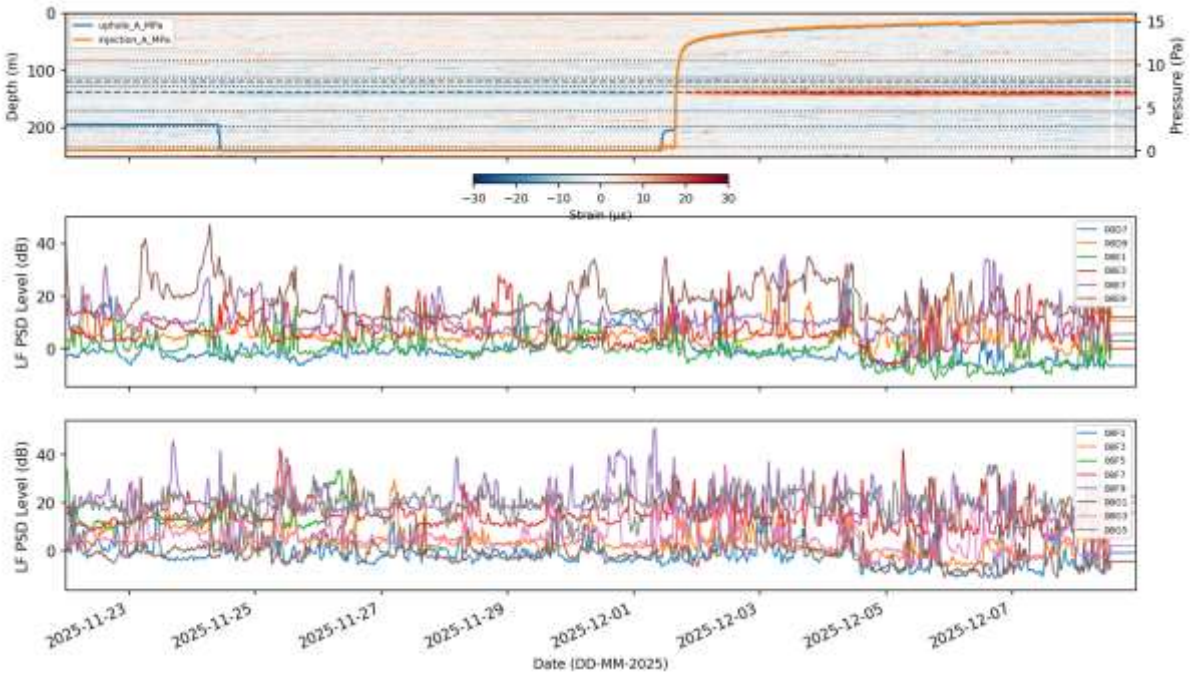

Figure 2-5: For MB8 borehole, combined fiber-optic sensing and pressure monitoring during fluid injection operations from November 23 to December 8, 2025. (Top) Distributed Strain Sensing (DSS) waterfall plot showing strain changes across depth (0 to 250 m) over time, overlaid with pressure profiles for the uphole (uphole_A_MPa, blue line) and injection (injection_A_MPa, orange line) locations. (Middle and Bottom) Distributed Acoustic Sensing (DAS) data showing Low-Frequency Power Spectral Density (LF PSD) levels (dB) over time across various channel locations (indicated by legends 08D7 to 08E9 and 08F1 to 08G5)

3 Self-potential analysis

In the context of fluid injection into fractured rock, SP signals arise primarily from two mechanisms: streaming potential, generated by fluid flow under a pressure gradient through the fracture network, and a thermoelectric contribution (Seebeck effect) when a temperature difference exists between the injected fluid and the host rock. A minor electrochemical contribution may also arise from salinity contrasts between the injection fluid and the formation water.

Figure 3-1 and Figure 3-2Figure 3-1 and show the mean SP anomaly per electrode for both injection cycles, presented as a phase-electrode summary matrix and as a spatial profile along the tunnel respectively. Both representations show the same pattern: a V-shaped minimum centered at ST1, with the largest negative anomalies at electrodes SE3 (S1, −2 m) and SE4 (N1, +2 m) flanking the injection borehole at equal distance, reaching −21 mV and −36 mV during Injection 2. The anomaly deepens from Injection 1 to Injection 2 at all electrodes close to ST1. A persistent asymmetry is observed between the two flanking electrodes — SE4 is consistently more negative than SE3 despite equal distance from ST1 — with the stronger response on the northward side. Electrode SE6 (N32, +35 m), located between ST1 and ST2, shows a positive anomaly of +33 mV during Injection 1 that is absent in Injection 2. The error bars in Figure 3-1 reflect the temporal variability of the 4h-median SP within each injection window, not measurement uncertainty; the narrow overlap between

Geo-INQUIRE is funded by the European Commission under project number 101058518 within the HORIZON-INFRA-2021-SERV-01 call

Injection 1 and Injection 2 at SE3 and SE4 confirms that the deepening is robust and not driven by a small number of outlier time steps.

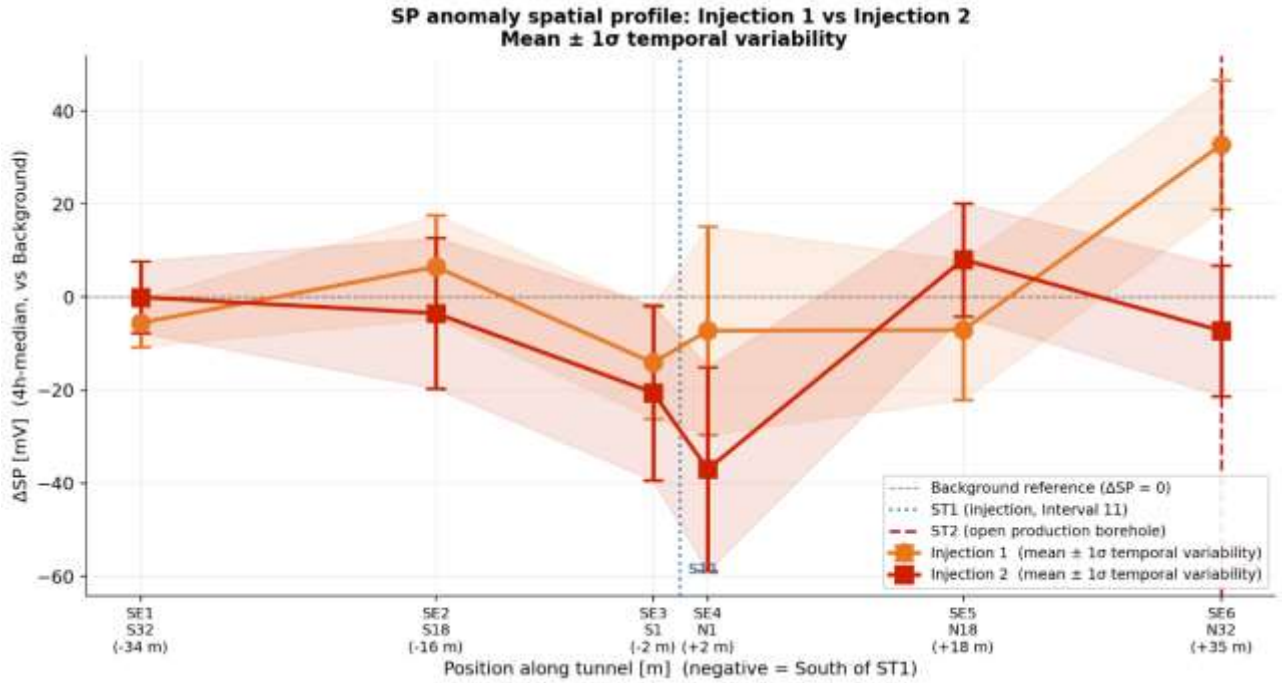

Figure 3-1: Mean SP anomaly ΔSP per electrode and injection cycle. ΔSP = 4h-median CMR-processed SP minus Background-phase mean. Electrodes SE1–SE6 sorted south to north relative to injection borehole ST1. Positive flow direction is southward toward the tunnel entrance. Steel blue dashed line = ST1 collar; red dashed line = ST2 collar.

The natural groundwater flow at the BedrettoLab is directed southward toward the tunnel entrance, which is the positive flow direction in the electrode coordinate system. The observed negative anomalies at SE3 and SE4 and the northward asymmetry favoring SE4 suggest a flow component directed toward ST2 that overprints the natural southward gradient during injection. The deepening of the anomaly between Injection 1 and Injection 2 may indicate progressive permeability enhancement between the two cycles, though further analysis is required. The positive anomaly at SE6 (N32, +35 m) during Injection 1, which is absent in Injection 2, may reflect a change in the local hydraulic gradient in the ST2 region; this could be consistent with fluid reaching the production borehole during the first cycle, or with a change in pressure distribution and connectivity between the two boreholes between cycles. Both interpretations remain preliminary.

Geo-INQUIRE is funded by the European Commission under project number 101058518 within the HORIZON-INFRA-2021-SERV-01 call

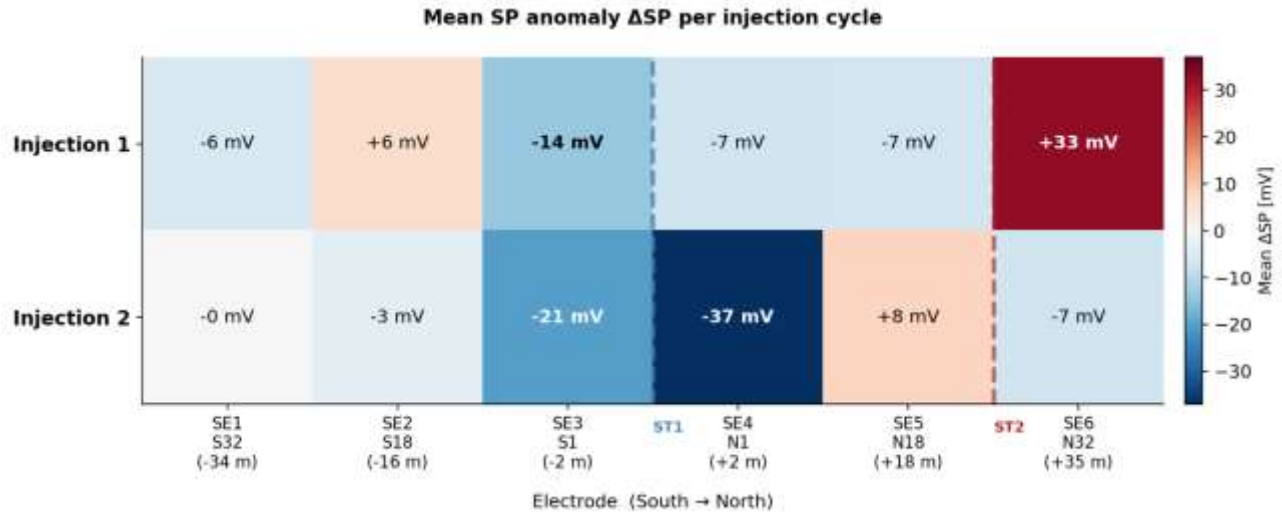

Figure 3-2: Mean SP anomaly ΔSP per electrode and injection cycle shown as a color matrix. ΔSP = 4h-median CMR-processed SP minus Background-phase mean. Electrodes SE1–SE6 sorted south to north relative to injection borehole ST1. Positive flow direction is southward toward the tunnel entrance. Steel blue dashed line = ST1 collar; red dashed line = ST2 collar.

3.1 SP and DTS

Figure 3-3 and Figure 3-4 show the relationship between the SP anomaly and the temperature anomaly ΔT measured by the DTS system in ST1 (channel 3, averaged over Interval 11 at 132–150 m depth) for both injection cycles.

Figure 3-3 shows scatter plots of ΔSP versus ΔT for electrodes SE3, SE4, and SE6, with linear regression lines indicating the apparent thermoelectric coupling coefficient C_T = ΔSP/ΔT. During Injection 1, C_T values are 2.3 mV/°C at SE3, 5.1 mV/°C at SE4, and 2.5 mV/°C at SE6. During Injection 2, values are lower and more uniform across the three electrodes, ranging between 1.8 and 2.3 mV/°C. The r^2 values are generally low to moderate (0.04–0.33), indicating a weak to moderate linear relationship between ΔT and ΔSP at the 4h timescale.

Geo-INQUIRE is funded by the European Commission under project number 101058518 within the HORIZON-INFRA-2021-SERV-01 call

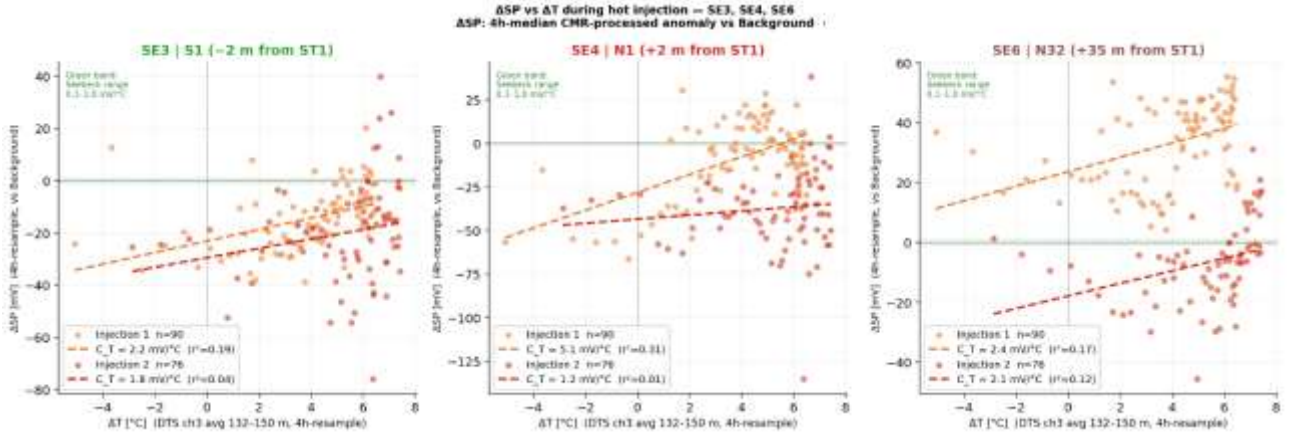

Figure 3-3: Scatter plots of SP anomaly ΔSP versus temperature anomaly ΔT for electrodes SE3, SE4, and SE6 during both injection cycles. ΔSP = 4h-median CMR-processed SP minus Background mean. ΔT = DTS channel 3 (ST1, down+up fibre paths averaged), averaged over Interval 11 (132–150 m depth), 4h-resample. Dashed lines = OLS regression. C_T = apparent thermoelectric coupling coefficient (slope). Green band = Seebeck prediction range for granite 0.1–1.0 mV/°C (Leinov et al., 2010; Revil et al., 2013).

Figure 3-4 shows the spatial profile of C_T along the tunnel for all six electrodes. During Injection 1, C_T increases from near zero at SE1 and SE2 on the southern side to a maximum of 5.1 mV/°C at SE4 just north of ST1, before decreasing toward SE6. During Injection 2, the profile is flatter and more symmetric, with values between 0 and 2.5 mV/°C across all electrodes.

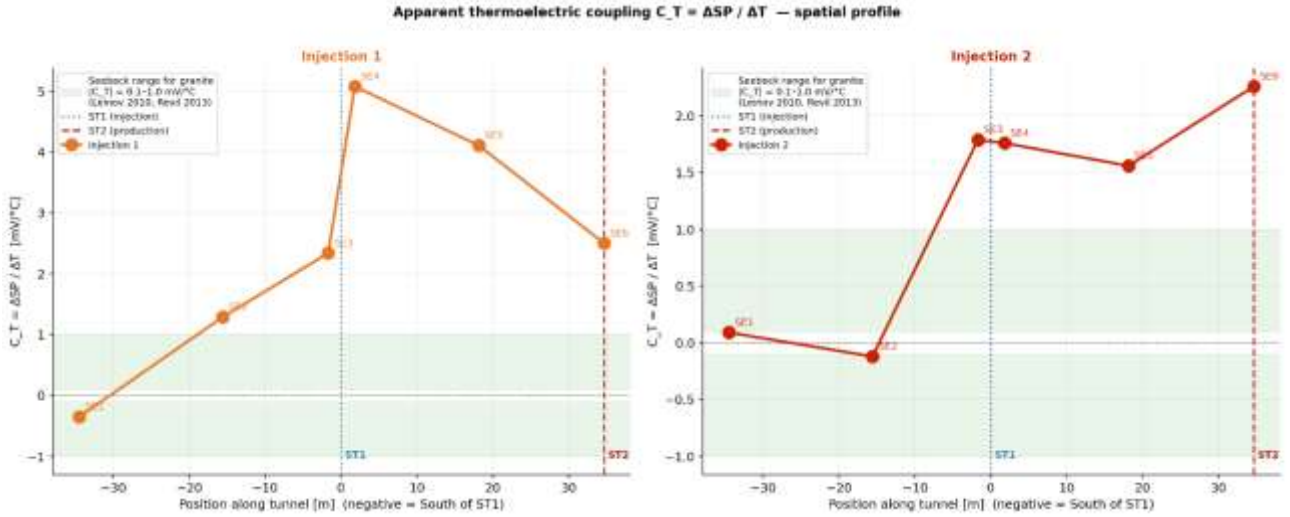

Figure 3-4: Spatial profile of apparent thermoelectric coupling coefficient C_T = ΔSP/ΔT along the tunnel for Injection 1 (orange) and Injection 2 (red). C_T computed as OLS slope of 4h-resampled ΔSP vs ΔT per electrode. ΔT from DTS channel 3 (ST1), Interval 11 (132–150 m depth). Green band = Seebeck prediction range for granite 0.1–1.0 mV/°C. Steel blue dotted line = ST1 collar; red dashed line = ST2 collar.

The measured C_T values exceed the predicted Seebeck range for granite of 0.1–1.0 mV/°C (Leinov et al., 2010; Revil et al., 2013), particularly during Injection 1. This suggests that the apparent coupling coefficient contains a significant streaming potential contribution in addition to any thermoelectric effect, as both mechanisms are active simultaneously during hot-water injection and cannot be separated from the current dataset alone. The northward asymmetry of the C_T profile during Injection 1, with higher values on the SE4 and SE5 side than on the SE3 and SE2 side, mirrors the asymmetry observed in the SP anomaly profile and is consistent with a preferential northward

flow component. The reduction in C_T values between Injection 1 and Injection 2, together with the flattening of the spatial profile, may reflect a change in the relative contributions of the two mechanisms or a change in the thermal gradient between cycles. Quantitative separation of streaming potential, thermoelectric, and electrochemical contributions remains ongoing work.

4 SP and seismicity

Although 92 induced seismic events were detected during Injection 1 and 65 during Injection 2, no systematic SP response could be identified at the individual event times (Figure 4-1). The occurrence of microseismic events is indicated by vertical lines, with line thickness and opacity scaled according to event magnitude. Despite periods of elevated seismic activity, none of the monitored electrodes (SE3, SE4, and SE7/B60) exhibit consistent SP peaks, polarity reversals, or transient anomalies that coincide with individual seismic events. Instead, the SP records are characterized by gradual variations evolving over several days. During both injection cycles, the observed SP anomalies develop progressively and show no clear temporal correspondence with individual induced seismic events. While the underlying mechanisms cannot be uniquely identified from these observations alone, the results suggest that the SP response is influenced by longer-term processes associated with the injection experiment rather than by direct responses to individual microseismic events.

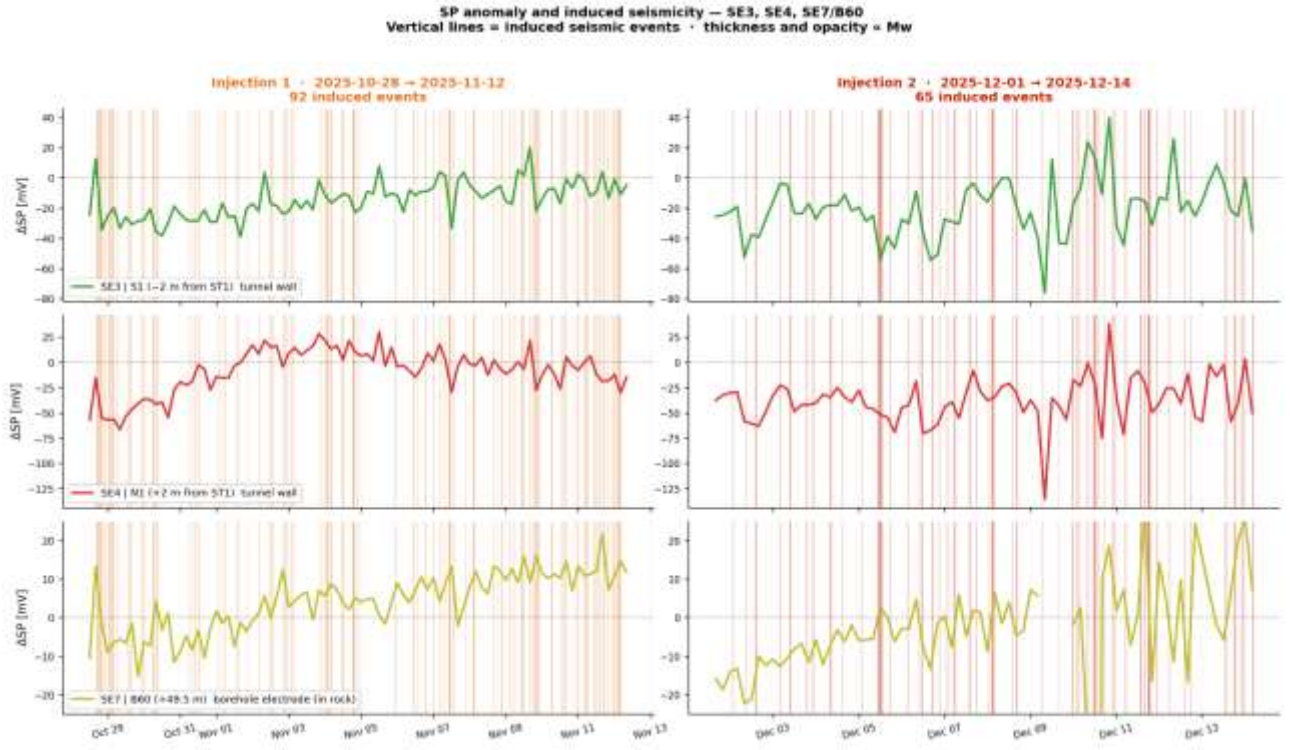

Figure 4-1: Temporal evolution of the 4-hour median SP anomaly (ΔSP) at electrodes SE3 (S1, −2 m from ST1), SE4 (N1, +2 m from ST1), and SE7/B60 (+49.5 m, borehole electrode) during Injection 1 (left) and Injection 2 (right). Vertical lines indicate induced seismic events, with line thickness and opacity proportional to event magnitude (Mw).

Geo-INQUIRE is funded by the European Commission under project number 101058518 within the HORIZON-INFRA-2021-SERV-01 call

5 Conference contribution

Results of this TA have been presented at the EGU annual meeting in Vienna, May 2026: Abstract: EGU26-9512 - Electric Self-Potential Measurements during Fluid Injection at the Bedretto Underground Laboratory by Nadine Haaf et al. Session ERE5.2 – Faults and fractures in geoenergy applications 1: Monitoring, laboratory and field work results.

EGU26-9512
EGU General Assembly 2026

Electric Self-Potential Measurements during Fluid Injection at the Bedretto Underground Laboratory

Nadine Haaf[1], Jeroma Azzola[1], Liliana Vargas Meleza[2], Marian Hertrich[2], Valentin Gischig[2], Mathilde Wimez[2], Antonio Pio Rinaldi[2], Fridolin Straub[2], Maren Brehme[2], Domenico Giardini[2], Francisco Sorbeto[3], and Andreas Alcolea[3]
[1]Karlsruhe Institute of Technology (KIT), Karlsruhe, Germany,
[2]ETH Zurich, Zurich, Swiss
[3]Geo-Energie Suisse, Zurich, Swiss

Self-potential (SP) monitoring was implemented at the Bedretto Underground Laboratory as part of the BEACH experiment to complement multi-parameter observations during fluid-injection tests. Continuous SP measurements have been conducted since the end of October 2025, with data acquired so far covering the period until mid-December, and monitoring planned to continue throughout the current year.

The SP setup consists of nine non-polarizable Pb/PbCl□ electrodes installed along the tunnel wall and within one borehole in the Mesozoic Crystalline Fault Zone. Tunnel-wall electrodes were placed in shallow drill holes and embedded using conductive contact material to ensure stable long-term coupling to the rock. A single electrode was installed in a 50m borehole to provide additional depth sensitivity. All electrodes were connected to a CR6 data logger, recording continuous SP time series with a sampling interval of one value per minute.

The recorded data span different operational phases, including background conditions as well as cold and warm water injection cycles and associated shut-in periods. This contribution presents an initial overview of the acquired SP dataset.

Note: Data, products, software and publications resulting from TA activities must be publicly accessible under a CC-BY 4.0, GPLv3 or equivalent open license. No embargos beyond June 2026 are allowed. They must cite Geo-INQUIRE as the source of funding. Minimal citation: "*Geo-INQUIRE is funded by the European Union (GA 101058518)*".